

*Research Paper*

## **A Numerical Analysis of Fluid-Structure Interaction Problem with a Flow Channel Embedded in a Structural Material**

P I JAGAD<sup>1</sup>, B P PURANIK<sup>2</sup> and A W DATE<sup>2</sup>

<sup>1</sup>Department of Mechanical Engineering, Institute of Technology, Nirma University, Ahmedabad 382481, India

<sup>2</sup>Department of Mechanical Engineering, Indian Institute of Technology Bombay, Powai, Mumbai 400 076, India

(Received on 06 February 2017; Revised on 08 May 2017; Accepted on 05 June 2017)

In the present work, numerical simulations have been performed on a model problem, representing a class of fluid-structure interaction problems. The model problem consists of a thin plate with a flow channel embedded in it. The governing equations for flow in the channel and displacement in plate structure are discretized using a finite volume procedure on unstructured meshes, and are solved in a one-way coupled manner with the flow in the channel influencing the stress field in the structure. The problem is presented in a generalized manner, in terms of the relevant dimensionless parameters obtained as part of the analysis. A parametric study is performed for the cases of isothermal and with heating of the fluid. The data from the parametric simulations are used to explain the stress field behavior in the solid plate, in response to independent dimensionless parameters. The overall methodology is presented in a manner that will be useful in analyzing any specific case of the class of fluid-structure interaction represented by the model problem.

**Keywords:** Flow Induced Stress; Fluid-Structure Interaction; One-Way Coupling; Stress Behavior

### **Introduction**

In thermo-fluid systems such as cooling of gas turbine blades, compact heat exchangers, electronics cooling, etc., a flowing fluid exerts forces (due to the pressure and viscous stresses) on the walls of the channels that are embedded within the structures, deforming them and inducing a stress field in the confining solid. Additionally, thermal stress can be induced in the solid in presence of temperature gradients. In most of the aforementioned thermo-fluid systems, the deformation of channel walls is small to be neglected, and hence the flow field can be assumed to be independent of the solid-body deformation. However, stress in the solid can be high, and depends on the properties of the fluid and flow conditions in addition to the properties of solid material. Therefore, while designing (from the strength point of view) these systems, fluid properties and the flow conditions should also be considered in addition to the properties of solid

material. For good/optimal design of such systems, it is important to be able to predict the stress behavior of structural materials in response to different flow conditions in a generalized manner, i.e., in terms of dimensionless parameters. This is the aim of present work. A model fluid-structure interaction problem consisting of a U-bend channel embedded in a thin plate is analyzed. The dimensionless parameters are derived and their effects on maximum value of dimensionless effective stress in the plate are studied and important conclusions are drawn. Two cases, excluding and including fluid heating, are considered.

An extensive literature survey of fluid-structure interaction problems did not show similar kind of work. Several of the reported studies involving interaction of a fluid with a solid focused on the solution approach such as partitioned method (Piperno *et al.*, 1995; Park *et al.*, 2001; Matthies and Steindorf, 2003; Degroote *et al.*, 2009; von Scheven and Ramm, 2011; Breuer

\*Author for Correspondence: E-mail: jagadp@yahoo.com, pankaj.jagad@nirmauni.ac.in

et al., 2012), monolithic method (Hubner et al., 2004; Etienne et al., 2006; Ryzhakov et al., 2010; Jog and Pal, 2011), unified single solution method (Greenshields and Weller 2005; Papadakis 2008), Arbitrary Lagrangian Eulerian (ALE) method (Hirt et al., 1974), Deforming Spatial Domain (DSD)/Stabilized Space Time (SST) method (Tezduyar et al., 1992; Tezduyar and Sathe, 2007; Takizawa and Tezduyar, 2011), Fictitious Domain (FD) (van Loon et al., 2007), Immersed Boundary Method (IBM) (Peskin, 1972; Peskin, 2002), method using interpolation operator (Gretarsson et al., 2011), full Eulerian fixed grid method (Takagi et al., 2012), and hybrid mesh free - Cartesian grid method (Yu et al., 2011). Other studies focused on the procedures employed for specific applications such as crystal growth process (Scheafer et al., 2002), fracture mechanics (Greenshields et al., 2002), blast wave mitigation (Peng et al., 2011), effect of pipe wall visco-elasticity during water hammer (Keramat et al., 2012), flow analysis of a ribbed helix lip seal (Wen et al., 2011), analysis of head-stack assembly in hard-disk drive (Kazemi, 2009), solution of an aero-elastic model describing the interactions of air flow with vocal folds (Svacek, 2011), dynamics of a cantilevered pipe aspirating fluid (Giacobbi et al., 2012), analysis of flexible turbo-machinery (Campbell and Paterson, 2011), analysis of flexible flapping airfoil (Unger et al., 2012), bio-mechanics and bioengineering applications (De Hart et al., 2003; Tang et al., 2003; Cheng et al., 2004).

In view of the fact that while the situation described in the model problem considered for the present study is relevant from practical applications mentioned earlier, and since there does not seem to be any such investigation reported in the literature, this work can be considered as a fundamental engineering analysis for such applications.

### Dimensionless Parameters of the Study

The schematic of the problem is shown in Fig. 1. For the purpose of illustration, the plate material is assumed to be elastic and following the von Mises yield criterion. However, it is noted that no special importance should be attached to this choice of model for computing limiting stress.

The equivalent stress (the von Mises stress) at a point in an elastic solid due to various forces acting on it is defined as

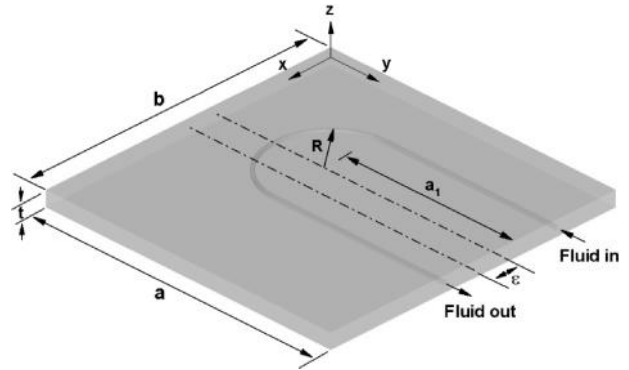


Fig. 1: Schematic of the flow in a channel embedded in a plate

$$\sigma_{eff} = \sqrt{0.5[(\sigma_{xx} - \sigma_{yy})^2 + (\sigma_{yy} - \sigma_{zz})^2 + (\sigma_{zz} - \sigma_{xx})^2] + 3(\sigma_{xy}^2 + \sigma_{yz}^2 + \sigma_{zx}^2)}, \quad (1)$$

where  $\sigma_{xx}$ ,  $\sigma_{xy}$ ,  $\sigma_{xz}$ , etc. are the components of the stress tensor  $\sigma_{ij}$ . A material starts yielding at a point where  $\sigma_{eff}$  reaches the yield strength. Hence, it is important to evaluate the maximum value of  $\sigma_{eff}$  ( $\sigma_{eff,max}$ ) and its location in a solid to know whether the material will yield or not under a given load condition, and the point of start of the yield.

### Dimensionless Representation of the Governing Equations and the Boundary Conditions

In order to understand the origin and significance of the dimensionless parameters of the problem, governing equations for the fluid flow and the plate, interface condition and the boundary conditions are expressed in dimensionless form as follows.

### Governing Equations

Assuming steady incompressible flow, the equations governing the transfer of mass and momentum and energy for a fluid flow, in Cartesian coordinate system, can be written as

$$\frac{\partial u_j}{\partial x_j} = 0, \quad (2)$$

$$\frac{\partial(\rho_f u_j u_i)}{\partial x_j} = -\frac{\partial p}{\partial x_i} + \frac{\partial}{\partial x_j} \left( \mu_f \frac{\partial u_i}{\partial x_j} \right), \quad (3)$$

$$\frac{\partial(\rho_f c_{p,f} u_j T)}{\partial x_j} = \frac{\partial}{\partial x_j} \left( k_f \frac{\partial T}{\partial x_j} \right), \quad (4)$$

where  $u_i$  is the component of the velocity vector  $u_j$  in the direction - i,  $\rho_f$  is the density of the fluid,  $\mu_f$  is the fluid dynamic viscosity,  $p$  stands for the fluid pressure,  $k_f$  is the thermal conductivity of the fluid,  $c_{p,f}$  is the specific heat of the fluid, and  $T$  is the temperature of the fluid. Assuming  $D_h$ ,  $\bar{u}$ , and  $\rho_f \bar{u}^2$  to be the characteristic length, velocity and pressure scales respectively and the fluid properties to be constant, Eqs. (2), (3), and (4) can be written in dimensionless form as

$$\frac{\partial u_j^*}{\partial x_j^*} = 0, \quad (5)$$

$$\frac{\partial (u_j^* u_i^*)}{\partial x_j^*} = -\frac{\partial (p/\rho_f \bar{u}^2)}{\partial x_i^*} + \frac{1}{Re} \frac{\partial^2 u_i^*}{\partial x_j^{*2}}, \quad (6)$$

$$\frac{\partial (u_j^* T^*)}{\partial x_j^*} = \frac{1}{Pe} \frac{\partial^2 T^*}{\partial x_j^{*2}}. \quad (7)$$

Here,  $\bar{u}$  is the average velocity of the fluid in the channel,  $D_h = 4A_c/P$  is the hydraulic diameter of the channel with  $A_c$  representing the area of cross section of the channel and  $P$  representing the perimeter of the channel cross section. Moreover,  $Re = \rho_f \bar{u} D_h / \mu_f$  is the flow Reynolds number and  $Pe = \rho_f c_{p,f} \bar{u} D_h / k_f$  is the Peclet number.

Governing steady state energy equation for a solid can be written as

$$\frac{\partial}{\partial x_j} \left( k_s \frac{\partial T}{\partial x_j} \right) = 0. \quad (8)$$

Here,  $T$  is the temperature of the solid and  $k_s$  is the thermal conductivity of the solid. Assuming the thermal conductivity to be constant, Eq. (7) can be written in the dimensionless form as

$$\frac{\partial^2 T^*}{\partial x_j^{*2}} = 0. \quad (9)$$

Neglecting the body force, the governing

equilibrium equation for an elastic solid can be written as

$$\frac{\partial (\sigma_{ij,s})}{\partial x_j} = \frac{\partial}{\partial x_j} \left[ \mu_s \left( \frac{\partial (\delta u_i)}{\partial x_j} + \frac{\partial (\delta u_j)}{\partial x_i} \right) + \lambda_s \frac{\partial (\delta u_k)}{\partial x_k} \delta_{ij} - (2\mu_s + 3\lambda_s) \alpha_s T \delta_{ij} \right] = 0 \quad (10)$$

where  $\delta u_i$  is the component of the displacement vector  $\delta u_j$  in the direction - i,  $\mu$  is the shear modulus,  $\lambda$  is the first Lamé's constant,  $\delta_{ij}$  is the Kronecker delta tensor,  $\alpha$  is the coefficient of thermal expansion of the solid,  $\sigma_{ij}$  is the stress tensor, and the subscript  $s$   $\sigma_{ij}$  stands for the solid. Assuming  $D_h$  to be the characteristic length scale, as well as, a reference scale for dimensionless representation of the displacement vector, and dividing Eq. (10) throughout by  $\rho_f \bar{u}^2$ , it can be written in the dimensionless form as:

$$\frac{\partial}{\partial x_j^*} \left[ \frac{\mu_s}{\rho_f \bar{u}^2} \left( \frac{\partial (\delta u_i^*)}{\partial x_j^*} + \frac{\partial (\delta u_j^*)}{\partial x_i^*} \right) + \frac{\lambda_s}{\rho_f \bar{u}^2} \frac{\partial (\delta u_k^*)}{\partial x_k^*} \delta_{ij} - \frac{(2\mu_s + 3\lambda_s)}{\rho_f \bar{u}^2} \frac{\alpha_s}{(k_f/q_w D_h)} T^* \delta_{ij} \right] = 0, \quad (11)$$

where,  $q_w$  is the heat flux supplied at the surface of the substrate.

### Interface Condition

At/across the fluid-solid interface there is continuity of temperature, the heat flux, the traction (force per unit area) and the velocity. The condition of the continuity of heat flux and temperature can be written as:

$$k_f \left( \frac{\partial T_i}{\partial n} \right)_f = k_s \left( \frac{\partial T_i}{\partial n} \right)_s \quad (12)$$

where,  $T_i$  is the temperature of the interface and  $\partial()/\partial n$  stands for the normal gradient. Subscripts  $f$  and  $s$  stand for the fluid and the solid domains respectively.

Equation (12) can be written in dimensionless form as:

$$\left( \frac{\partial T_i^*}{\partial n^*} \right)_f = \frac{k_s}{k_f} \left( \frac{\partial T_i^*}{\partial n^*} \right)_s \quad (13)$$

The condition of continuity of the traction is expressed as:

$$(\sigma_{ij}n_j)_f = (\sigma_{ij}n_j)_s, \quad (14)$$

where  $n_j$  is the outward facing normal to the interface. Substituting for the stress tensor in Eq. (14) using the relevant constitutive relations

$$\begin{aligned} & -p\delta_{ij}n_j + \mu_f \left( \frac{\partial u_i}{\partial x_j} + \frac{\partial u_j}{\partial x_i} \right) n_j \\ & = \mu_s \left[ \frac{\partial(\delta u_i)}{\partial x_j} + \frac{\partial(\delta u_j)}{\partial x_i} \right] n_j \\ & + \lambda_s \frac{\partial(\delta u_k)}{\partial x_k} \delta_{ij}n_j - (2\mu_s + 3\lambda_s)\alpha_s T \delta_{ij}n_j \end{aligned} \quad (15)$$

The pressure can be expressed as  $p = p_{out} + \Delta p$  where,  $p_{out}$  and  $\Delta p$  stand for the channel outlet pressure and pressure drop respectively. Therefore, invoking the identity  $\delta_{ij}n_j = n_i$

$$\begin{aligned} & -[p_{out} + \Delta p]n_i + \mu_f \left( \frac{\partial u_i}{\partial x_j} + \frac{\partial u_j}{\partial x_i} \right) n_j \\ & = \mu_s \left[ \frac{\partial(\delta u_i)}{\partial x_j} + \frac{\partial(\delta u_j)}{\partial x_i} \right] n_j + \lambda_s \frac{\partial(\delta u_k)}{\partial x_k} n_i \\ & - (2\mu_s + 3\lambda_s)\alpha_s T n_i \end{aligned} \quad (16)$$

Equation (16) can be written in the dimensionless form as:

$$\begin{aligned} & - \left[ \frac{p_{out}}{\rho_f \bar{u}^2} + \frac{\Delta p}{\rho_f \bar{u}^2} \right] n_i + \frac{1}{Re} \left( \frac{\partial u_i^*}{\partial x_j^*} + \frac{\partial u_j^*}{\partial x_i^*} \right) n_j \\ & = \frac{\mu_s}{\rho_f \bar{u}^2} \left[ \frac{\partial(\delta u_i^*)}{\partial x_j^*} + \frac{\partial(\delta u_j^*)}{\partial x_i^*} \right] n_j \end{aligned}$$

$$+ \frac{\lambda_s}{\rho_f \bar{u}^2} \frac{\partial(\delta u_k^*)}{\partial x_k^*} n_i - \frac{(2\mu_s + 3\lambda_s)}{\rho_f \bar{u}^2} \frac{\alpha_s}{(k_f/q_w D_h)} T^* n_i \quad (17)$$

Since the convection/velocity is neglected in the plate in the present work, the condition of continuity of velocity at the fluid-solid interface is redundant.

### Boundary Conditions

Uniform velocity and temperature of the fluid at the channel inlet is assumed. Therefore,

$$u_{i,B}^* = u_{i,in}^*, \quad (18)$$

and

$$T_B^* = T_{f,in}^*, \quad (19)$$

with subscript  $B$  representing the boundary surface,  $u_{i,in}$  and  $T_{f,in}$  representing the specified value of the velocity vector and the fluid temperature respectively at the inlet.

Zero normal gradient of the flow variables and temperature at the channel outlet is assumed. Hence,

$$\left( \frac{\partial \phi^*}{\partial n^*} \right)_B = 0, \quad (20)$$

where  $\phi$  stands for  $u_i$ ,  $p$ , and  $T$ .

The plate is assumed to be constrained at the external boundaries. Therefore,

$$\delta u_{i,B}^* = 0. \quad (21)$$

A symmetry plane passing through the thickness of the plate is assumed. Therefore,

$$\delta u_{n,B}^* = 0 \quad (22)$$

and

$$\left[ \frac{\partial(\delta u_t^*)}{\partial n^*} \right]_B = 0, \quad (23)$$

where, the subscripts  $n$  and  $t$  stand for the normal and tangential component respectively.

Assume that the fluid is heated by supplying a constant heat flux of  $q_w$  at the two surfaces of the plate and the edges of the plate are in contact with an ambient air at a temperature  $T_a$  and the heat transfer coefficient for the convective heat transfer to the air is  $h_a$ . Therefore,

$$\frac{k_s}{k_f} \left( \frac{\partial \left( T / (q_w D_h / k_f) \right)}{\partial n^*} \right)_B = 1, \quad (24)$$

and

$$\frac{k_s}{k_f} \left( \frac{\partial \left( T / (q_w D_h / k_f) \right)}{\partial n^*} \right)_B = \frac{h_a}{(k_f / D_h)} \frac{(T_B - T_a)}{(q_w D_h / k_f)}. \quad (25)$$

From the interface condition (Eq. (17),) it can be observed that the stress in the plate is induced due to three types of forces at the interface explained as follows. Considering the limiting case of the flow velocity tending to zero, there will be uniform pressure distribution equal to  $p_{out}/\rho_f \bar{u}^2$  throughout the channel. This will cause a static force acting on the channel wall inducing a stress  $\sigma_{ij,s}/\rho_f \bar{u}^2$ , which will be a function of  $p_{out}/\rho_f \bar{u}^2$  alone. Now, as the fluid starts flowing through the channel, the uniform pressure  $p_{out}/\rho_f \bar{u}^2$  will be appended with a pressure distribution corresponding to  $\Delta p/\rho_f \bar{u}^2$ , which is a function of  $Re$ . Now, the appended pressure distribution and the viscous stress ( $1/Re$ ) ( $\partial u_i^*/\partial x_j^* + \partial u_j^*/\partial x_i^*$ ) will induce an additional stress in the plate, which will be a function of  $Re$  as well as  $p_{out}/\rho_f \bar{u}^2$ . From the foregoing analysis, for a given geometry/dimensions of the plate and that of the channel, the dimensionless stress solution in the plate can be expressed as:

$$\frac{\sigma_{ij,s}}{\rho_f \bar{u}^2} =$$

$$f \left( \frac{E}{\rho_f \bar{u}^2}, \nu, \frac{p_{out}}{\rho_f \bar{u}^2}, \frac{\Delta p}{\rho_f \bar{u}^2}, Re, \frac{k_s}{k_f}, Pe, \frac{\alpha_s}{(k_f/q_w D_h)}, \frac{T_a - T_{f,in}}{(q_w D_h/k_f)}, \frac{h_a}{(k_f/D_h)} \right) \quad (26)$$

Moreover, we can write (Jagad *et al.*, 2015)

$$\frac{\Delta p}{\rho_f \bar{u}^2} = f_1(Re). \quad (27)$$

Hence, Eq. (27) can be rewritten as:

$$\frac{\sigma_{ij,s}}{\rho_f \bar{u}^2} =$$

$$f_2 \left( \frac{E}{\rho_f \bar{u}^2}, \nu, \frac{p_{out}}{\rho_f \bar{u}^2}, Re, \frac{k_s}{k_f}, Pe, \frac{\alpha_s}{(k_f/q_w D_h)}, \frac{T_a - T_{f,in}}{(q_w D_h/k_f)}, \frac{h_a}{(k_f/D_h)} \right) \quad (28)$$

### Parametric Study Excluding Heating of the Fluid

Consider the model problem shown in Fig. 1. The plate is assumed to be of the dimensions  $a = b = 50\text{mm}$ ,  $t = 2.5\text{mm}$ . The cross-section of channel is assumed to be  $0.5\text{ mm} \times 0.5\text{ mm}$ . The channel is assumed to be placed symmetrically ( $\varepsilon = 0$ ) in the plate. The dimensions  $R = 10\text{mm}$  and  $a_1 = 30\text{ mm}$  are assumed. When heating is excluded, Eq. (28) can be rewritten as:

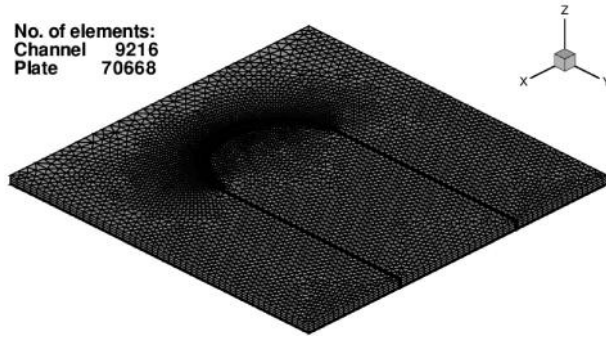
$$\frac{\sigma_{ij,s}}{\rho_f \bar{u}^2} = f_2 \left( \frac{E}{\rho_f \bar{u}^2}, \nu, \frac{p_{out}}{\rho_f \bar{u}^2}, Re \right). \quad (29)$$

The functional relationship given by Eqs. (29) is studied. The values of the parameters employed for the study are summarized in Table 1. The Poisson's ratio  $\nu = 0.17$  represents silicon,  $\nu = 0.3$  represents metal such as steel, and  $\nu = 0.37$  represents polymer material Polycarbonate. Fairly wide range of  $E/\rho_f \bar{u}^2$  and  $p_{out}/\rho_f \bar{u}^2$  is employed.

For simulations, the symmetry in  $z$ -direction (along the thickness) is considered. The unstructured mesh finite volume procedure (Jagad *et al.*, 2011) is employed for solving the problem. The mesh employed is shown in Fig. 2. The flow domain through the channel is discretized using a hexahedral mesh and the domain in the plate is discretized using a hybrid

**Table 1: Values of the parameters for stress behavior study when heating of the fluid is excluded**

Parameter	Values
Re	292, 380, 468, 585, 877, 1170, 1460, 1750, 2050
$E/\rho_f \bar{u}^2$	$1.88 \times 10^5$ , $2.56 \times 10^5$ , $3.68 \times 10^5$ , $5.75 \times 10^5$ , $1.02 \times 10^6$ , $2.3 \times 10^6$ , $9.2 \times 10^6$
$\nu$	0.17, 0.3, 0.37
$p_{out}/\rho_f \bar{u}^2$	0, 5, 10, 15, 20, 25, 30, 35, 40, 45, 50, 60, 70, 80, 90, 100, 200 300, 500, 1000, 2000, 3000, 4000, 5000

**Fig. 2: The mesh employed for the simulations for stress behavior study**

mesh consisting of hexahedral and triangular prismatic cells.

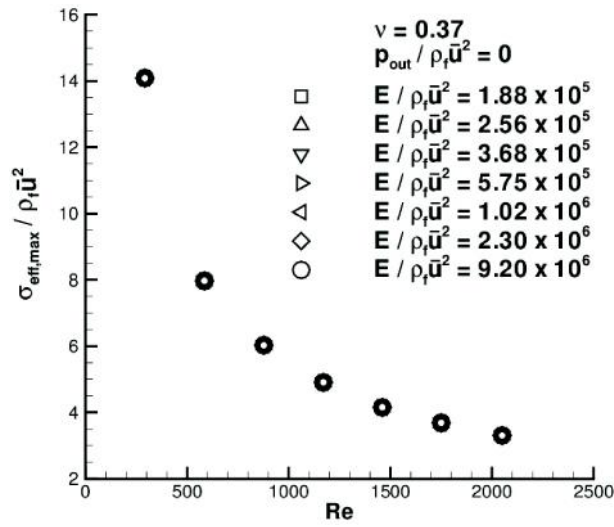
The behavior of  $\sigma_{eff,max}/\rho_f \bar{u}^2$  as a function of  $Re$  for different values of  $E/\rho_f \bar{u}^2$  is shown in Fig. 3. The collapsing plots imply redundancy of the parameter  $E/\rho_f \bar{u}^2$ . Figure 4 shows the behavior of  $\sigma_{eff,max}/\rho_f \bar{u}^2$  as a function of  $p_{out}/\rho_f \bar{u}^2$  for  $Re$  varying from 292 to 2050 and  $\nu = 0.17$  and 0.3. It can be observed that  $\sigma_{eff,max}/\rho_f \bar{u}^2$  drops with rise in  $Re$  since the dimensionless pressure drop  $\Delta p/\rho_f \bar{u}^2$  (see Fig. 6) and the dimensionless viscous stress  $(\partial u_i^*/\partial x_j^* + \partial u_j^*/\partial x_i^*)$  at the channel wall decrease. Moreover, the effect of  $Re$  on  $\sigma_{eff,max}/\rho_f \bar{u}^2$  is smaller at higher  $p_{out}/\rho_f \bar{u}^2$  since the fluid static pressure

becomes dominant and the  $\Delta p/\rho_f \bar{u}^2$  becomes insignificant. With the rise in  $p_{out}/\rho_f \bar{u}^2$ , force due to static pressure on the channel walls increases leading to the rise in the dimensionless stress  $\sigma_{eff,max}/\rho_f \bar{u}^2$  in the plate material. In order to convey the effect of  $\nu$  on  $\sigma_{eff,max}/\rho_f \bar{u}^2$  clearly, an extract from Fig. 4 is shown in Fig. 5. As  $\nu$  increases,  $\sigma_{eff,max}/\rho_f \bar{u}^2$  decreases. As  $\nu$  increases, the maximum value of the shear stress components decrease and that of the normal stress components increases. As a result, the maximum value of  $\sigma_{eff,max}/\rho_f \bar{u}^2$  decreases due to the dominant contribution of shear stress components. The percentage change in the value of  $\sigma_{eff,max}/\rho_f \bar{u}^2$  with  $\nu$  is found to be almost constant for different values of  $Re$  as well as  $p_{out}/\rho_f \bar{u}^2$ .

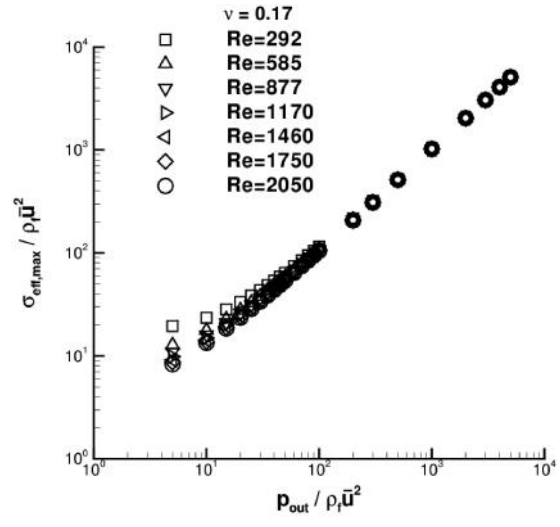
A few contour plots in a plane at  $z = 0.1875$  mm are shown in Figs. 7-8. Water ( $\rho = 1000$  kg/m<sup>3</sup> and  $\mu = 8.55 \times 10^{-4}$  Pa-s) is assumed to be the fluid passing through the channel. From these plots, it can be observed that the point of maximum effective stress is either in the vicinity of channel inlet or near the end of left limb of the channel depending on the range of parameters, as already stated earlier.

### Parametric Study Including Heating of the Fluid

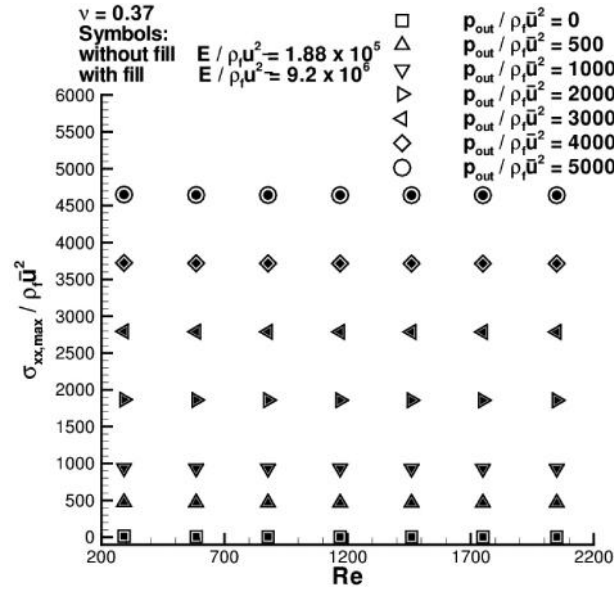
In the present case, for given dimensions of the plate and channel, and fixed  $T_a$ ,  $T_{f,in}$  and  $h_a$ , Eq. (28) can be rewritten as:



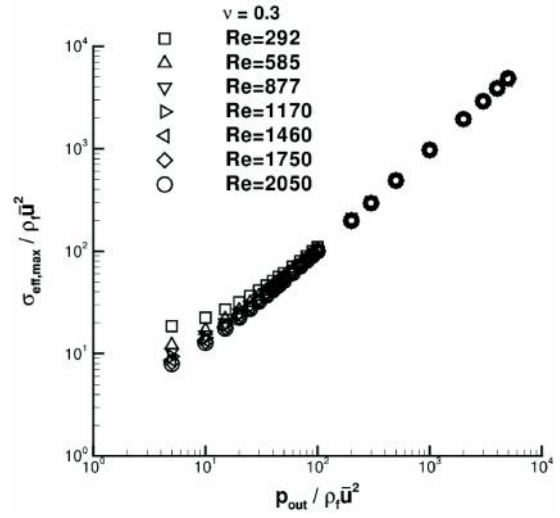
(a)  $P_{out} / \rho_f \bar{u}^2 = 0$



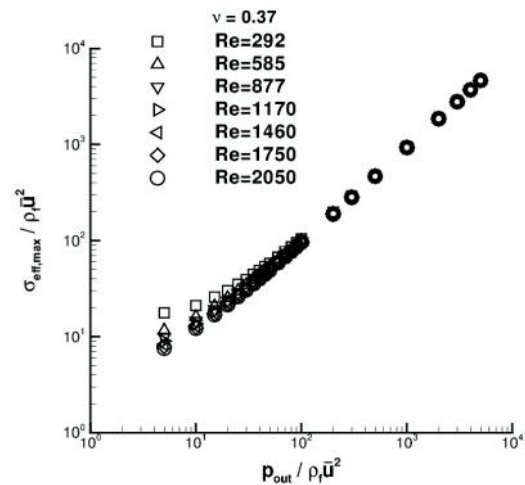
(a)  $\nu = 0.17$



(b) For different values of  $P_{out} / \rho_f \bar{u}^2$



(b)  $\nu = 0.3$



(c)  $\nu = 0.37$

Fig. 3: Behavior of  $\sigma_{eff,max} / \rho_f \bar{u}^2$  as a function of  $Re$  for different values of  $E / \rho_f \bar{u}^2$  showing redundancy of  $E / \rho_f \bar{u}^2$

$$\frac{\sigma_{eff,max}}{\rho_f \bar{u}^2} = G_1 \left( \frac{E}{\rho_f \bar{u}^2}, \nu, Re, \frac{P_{out}}{\rho_f \bar{u}^2}, \frac{k_s}{k_f}, Pe, \left( \frac{\alpha_s}{k_f / q_w D_h} \right) \right). \quad (30)$$

The problem described in Sec. 3 is now studied assuming heating of the fluid. The functional relationship given in Eq. (30) is studied. The effects

Fig. 4: Behavior of  $\sigma_{eff,max} / \rho_f \bar{u}^2$  as a function of  $P_{out} / \rho_f \bar{u}^2$  for different values of  $Re$  and  $\nu$

of  $Re$ ,  $E/\rho_f \bar{u}^2$ ,  $\nu$ ,  $k_s/k_f$ ,  $Pe$  and  $\alpha_s/(k_f/q_w D_h)$  on

**Table 2: Values of the parameters for a case when heating of the fluid is considered**

$Re$	292, 877, 1460, 2050
$E/\rho_f \bar{u}^2$	$1.88 \times 10^5$ , $9.2 \times 10^6$
$\nu$	0.3, 0.37
$k_s/k_f$	0.3, 350
$Pe$	200, 10000
$\alpha_s/(k_f/q_w D_h)$	$1.2 \times 10^{-7}$ , $1.2 \times 10^{-5}$

$\sigma_{eff,max}/\rho_f \bar{u}^2$  are determined. For the present study,  $p_{out}/\rho_f \bar{u}^2 = 0$  is assumed. The values of different parameters used for the study are summarized in Table 2.

The symmetry of the problem in  $z$ -direction (along the thickness of the plate) is considered. A uniform velocity and temperature of the fluid are assumed at the channel inlet. At the channel outlet, normal gradients of the flow variables and that of the

fluid temperature are assumed to be zero. No-slip boundary condition is employed on the channel walls. All external boundaries of the plate are assumed to be fixed. Continuity of the traction (force per unit area), velocity, temperature and heat flux are implemented at the channel walls. Uniform heat flux condition is assumed at the top and bottom surfaces of the plate. At the edges of the plate, natural convection heat transfer to the ambient air is assumed.

A solution procedure similar to (Jagad et al., 2011) is used. For simultaneous determination of the fluid and solid temperature fields, the procedure described in (Jagad et al., 2012) is used. The same mesh as that shown in Fig. 2 and described in Sec. 3 is used.

The effects of the aforementioned parameters on  $\sigma_{eff,max}/\rho_f \bar{u}^2$  are shown in Figs. 9-10. It is found that  $Re$  does not affect  $\sigma_{eff,max}/\rho_f \bar{u}^2$  for larger values of  $\alpha_s/(k_f/q_w D_h)$  and  $E/\rho_f \bar{u}^2$  because the thermal stresses (due to the temperature distribution in the plate) are the predominant contributors and are not dependent on  $Re$ . At lower values of  $\alpha_s/(k_f/q_w D_h)$  and  $E/\rho_f \bar{u}^2$ , the contribution of mechanical stresses (due to the forces on channel walls due to the fluid pressure and viscous effect) becomes equivalent and

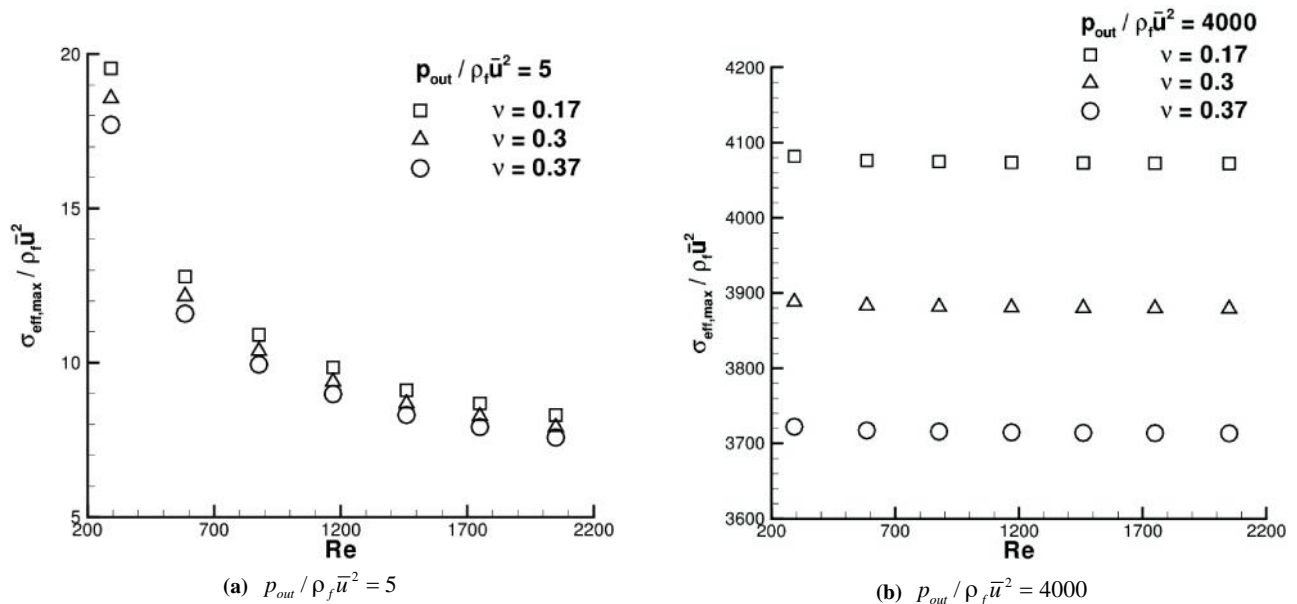


**Fig. 5: Behavior of  $\sigma_{eff,max}/\rho_f \bar{u}^2$  as a function of  $Re$  for different values of  $\nu$ , showing the effect of  $\nu$**

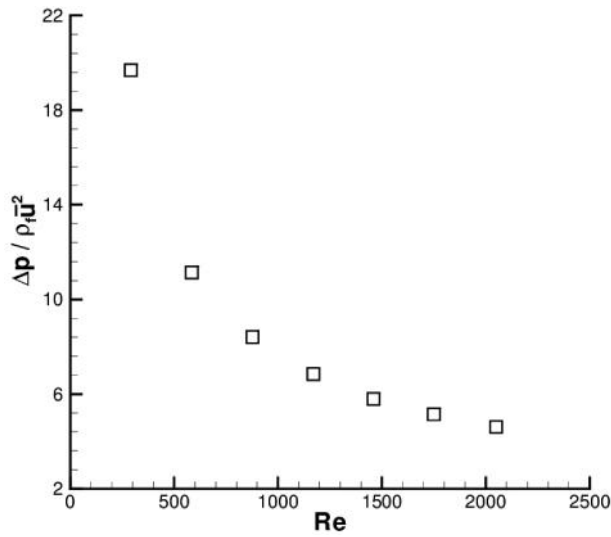


Fig. 6: Dimensionless pressure drop  $\Delta p / \rho_f \bar{u}^2$  as a function of  $Re$

$\sigma_{eff,max} / \rho_f \bar{u}^2$  slightly increases with increase in  $Re$ . As  $Pe$  or  $k_s/k_f$  increases,  $\sigma_{eff,max} / \rho_f \bar{u}^2$  decreases because temperature gradients in the plate decrease, hence, the thermal stress decreases. The percentage change in  $\sigma_{eff,max} / \rho_f \bar{u}^2$  with  $Pe$  is found to be more for larger  $k_s/k_f$  and  $\nu$ , and smaller  $E/\rho_f \bar{u}^2$  and

$\alpha_s / (k_f/q_w D_h)$ . Similarly, the percentage change in  $\sigma_{eff,max} / \rho_f \bar{u}^2$  with  $k_s/k_f$  is found to be more for larger  $Pe$  and  $\nu$ , and smaller  $E/\rho_f \bar{u}^2$  and  $\alpha_s / (k_f/q_w D_h)$ . As  $E/\rho_f \bar{u}^2$  or  $\alpha_s / (k_f/q_w D_h)$  or  $\nu$  increases  $\sigma_{eff,max} / \rho_f \bar{u}^2$  increases because thermal stress increases in the plate.

**Conclusions**

A model problem of determination of stress behavior of the confining structure in response to different flow conditions in an internal flow situation consisting of a U-bend channel embedded in a thin plate is analyzed here. Two cases, without and with the fluid heating, are considered. The dimensionless governing parameters are derived. The effects of these parameters on maximum value of dimensionless effective stress in the plate material are studied.

In the first case, when heating of fluid is not considered, the following conclusions are derived:

- The effect of a dimensionless Young’s modulus on the dimensionless maximum effective stress is found to be insignificant over a wide range of the parameters.

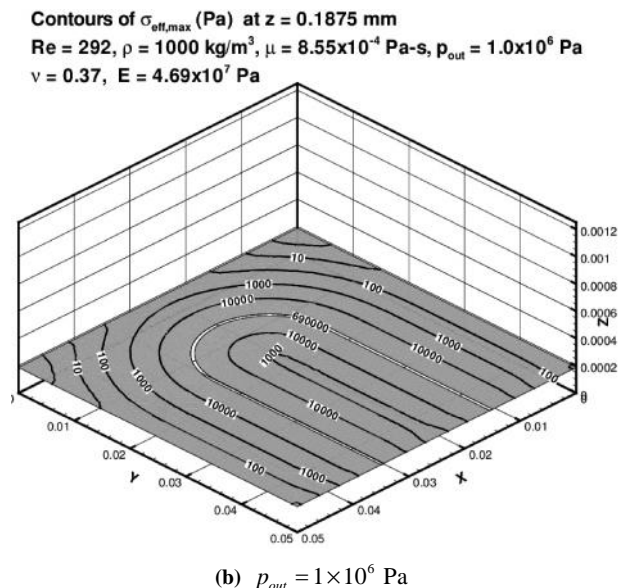
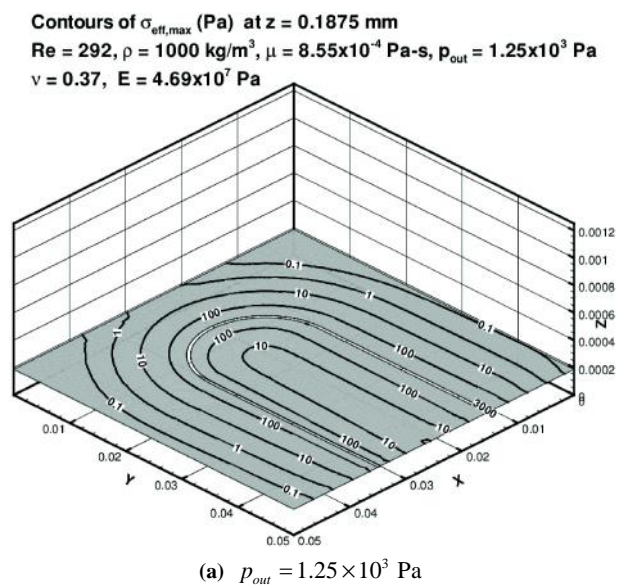


Fig. 7: Contours of  $\sigma_{eff,max}$  (Pa) for the stress behavior study at  $z = 0.1875$  mm,  $Re = 292, \rho = 1000 \text{ kg/m}^3, \mu = 8.55 \times 10^{-4} \text{ Pa-s}, \nu = 0.37, E = 4.69 \times 10^7 \text{ Pa}$

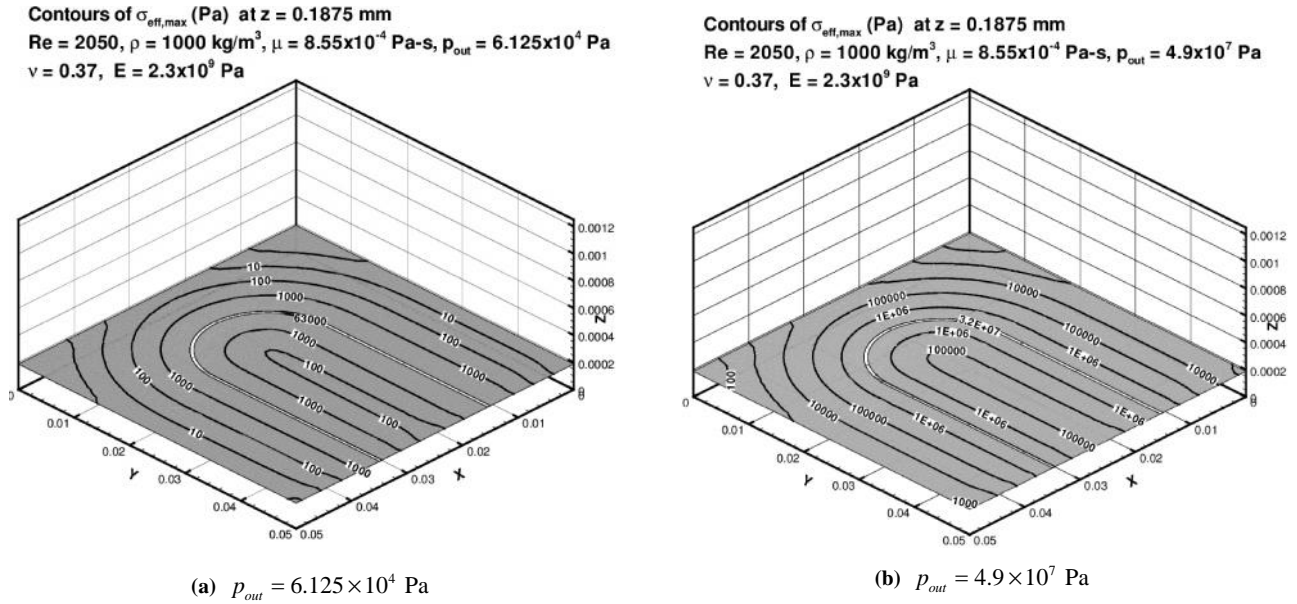


Fig. 8:  $\sigma_{eff,max}$  (Pa) for the stress behavior study at  $z = 0.1875$  mm,  $Re = 2050, \rho = 1000 \text{ kg/m}^3, \mu = 8.55 \times 10^{-4} \text{ Pa-s}, \nu = 0.37, E = 4.69 \times 10^9 \text{ Pa}$

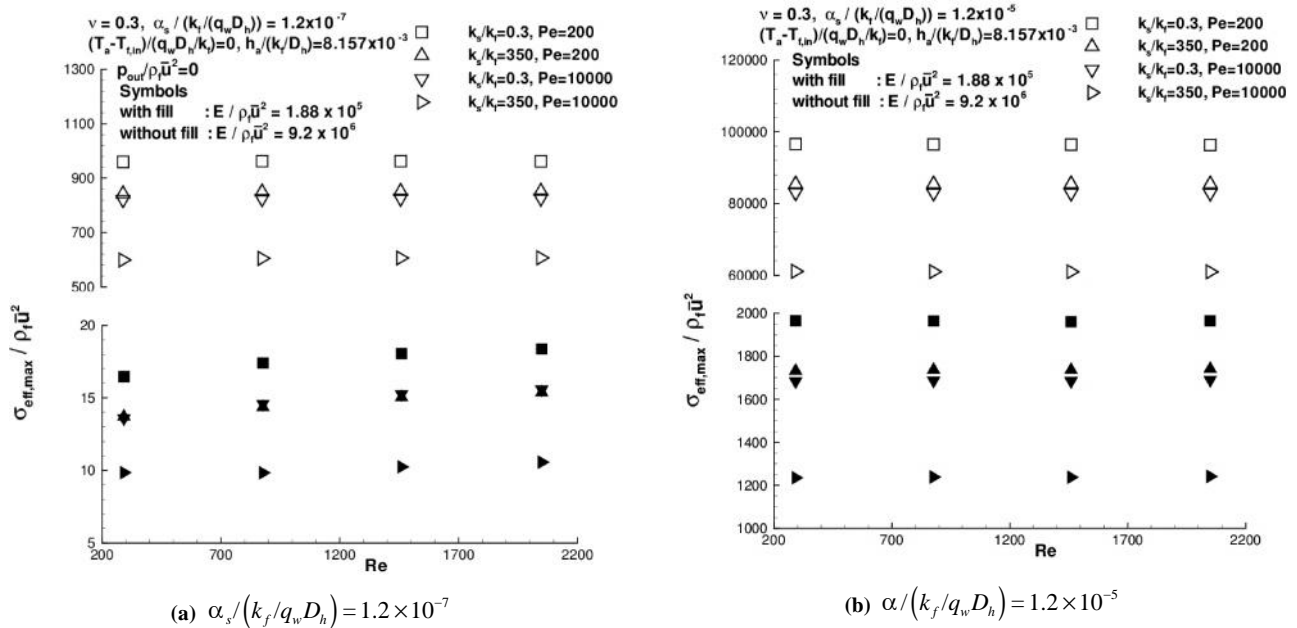


Fig. 9: Effects of the parameters on  $\sigma_{eff,max} / \rho_f \bar{u}^2$  for a case when fluid heating is included and  $\nu = 0.3$

- The dimensionless stress is found to decrease with increase in the flow Reynolds number. The effect of the flow Reynolds number on dimensionless maximum effective stress is found to become less significant with increase in the dimensionless static pressure at the channel outlet. At high values of dimensionless static

pressure at the channel outlet (say  $\geq 500$ ), dimensionless pressure drop becomes insignificant as compared to static pressure of the fluid in the channel. Hence, the effect of the flow Reynolds number also becomes insignificant.

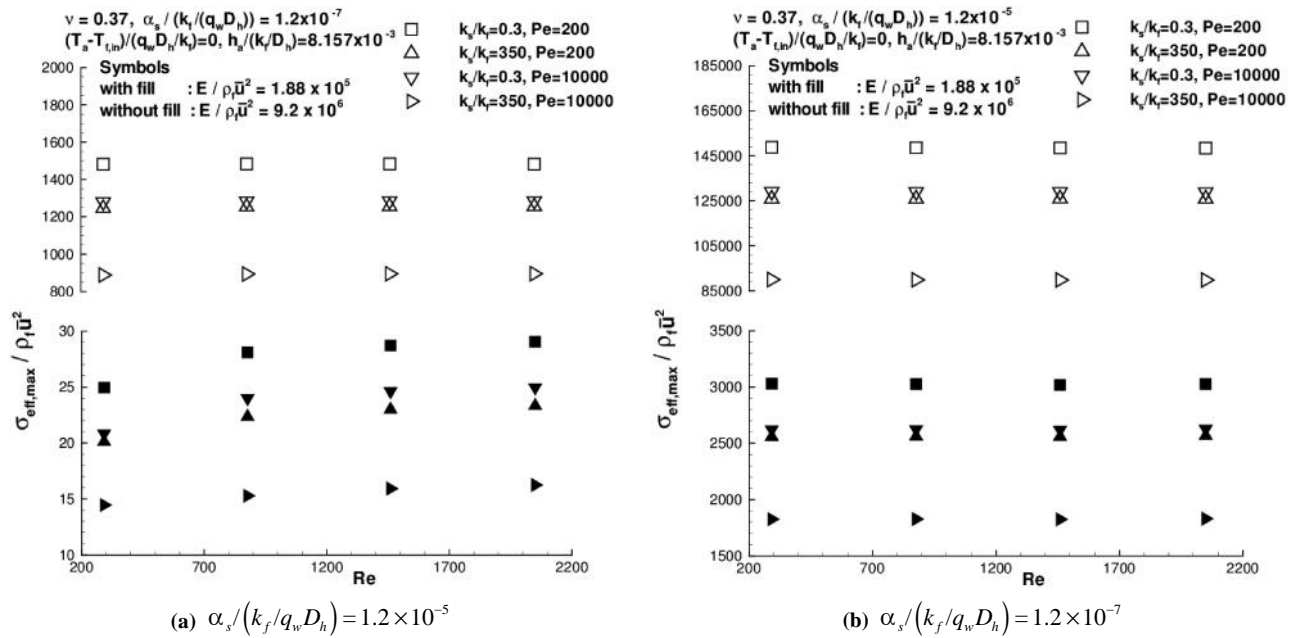


Fig. 10: Effects of the parameters on  $\sigma_{eff,max}/\rho_f \bar{u}^2$  for a case when fluid heating is included and  $\nu = 0.37$

- The dimensionless maximum effective stress is found to decrease with increase in the Poisson’s ratio.

For the second case, when heating of the fluid is considered the conclusions derived are as follows:

- At higher values of dimensionless coefficient of thermal expansion and dimensionless Young’s modulus the thermal stress is found to be predominant over mechanical stress. Hence, the effect of the flow Reynolds number on dimensionless maximum effective stress is found to be insignificant at higher values of the dimensionless coefficient of thermal expansion and the dimensionless Young’s modulus.
- The dimensionless maximum effective stress is found to decrease with increase in the flow

Pelet number or the conductivity ratio due to the decrease in temperature gradients in the plate.

- Unlike in the first case, in the second case the dimensionless Young’s modulus is found to affect the dimensionless maximum effective stress. With increase in the dimensionless Young’s modulus or the dimensionless coefficient of thermal expansion or Poisson’s ratio the dimensionless maximum effective stress is found to increase due to increase in the thermal stress.

While the foregoing conclusions are specific to the model problem analyzed in this work, an overall methodology is presented in a general framework, and is considered to be useful for the class of fluid-structure situations exemplified by the model problem.

### References

Breuer M, De Nayer G, Munsch M, Gallinger T and Wuchner R (2012) Fluid-structure interaction using a partitioned semi-implicit predictor-corrector coupling scheme for the application of large-eddy simulation in *J Fluid Struct* **29** 107-130

Campbell R L and Paterson E G (2011) Fluid-structure interaction

analysis of flexible turbomachinery in *J Fluid Struct* **27** 1376-1391

Cheng R, Lai Y G and Chandran K B (2004) Three-dimensional fluid-structure interaction simulation of bileaflet mechanical heart valve flow dynamics in *Ann Biomed Eng* **32** 1471-1483

Degroote J, Bathe K J and Vierendeels J (2009) Performance of a

- new partitioned procedure versus a monolithic procedure in fluid-structure interaction in *Comput Struct* **87** 793-801
- De Hart J, Peters G W M, Schreurs P J G and Baaijens F P T (2003) A three-dimensional computational analysis of fluid-structure interaction in the aortic valve in *J Biomech* **36** 103-112
- Etienne S, Pelletier D and Garon A (2006) A monolithic formulation for unsteady fluid-structure interactions In: Collection of Technical Papers - 44th AIAA Aerospace Sciences Meeting **11** 8301-8313
- Giacobbi D B, Rinaldi S, Semler C and Paidoussis M P (2012) The dynamics of a cantilevered pipe aspirating fluid studied by experimental, numerical and analytical methods in *J Fluid Struct* **30** 73-96
- Greenshields C J, Venizelos G P and Ivankovic A (2000) A fluid-structure model for fast brittle fracture in plastic pipes in *J Fluid Struct* **14** 221-234
- Greenshields C J and Weller H G (2005) A unified formulation for continuum mechanics applied to fluid-structure interaction in flexible tubes in *Int J Numer Meth Eng* **64** 1575-1593
- Greтарыsson J T, Kwatra N and Fedkiw R (2011) Numerically stable fluid-structure interactions between compressible flow and solid structures in *J Comput Phys* **230** 3062-3084
- Hirt C W, Amsden A A and Cook J L (1974) An arbitrary lagrangian-eulerian computing method for all flow speeds in *J Comput Phys* **14** 227-253
- Hubner B, Walhorn E and Dinkler D (2004) A monolithic approach to fluid-structure interaction using space-time finite elements and Computer Methods in *Appl Mech Eng* **193** 2087-2104
- Jagad P I, Puranik B P and Date A W (2011) A finite volume procedure on unstructured meshes for fluid-structure interaction problems in *World Academy of Science Engineering and Technology* **79** 639-645
- Jagad P, Puranik B and Date A (2012) An iterative procedure for the evaluation of a conjugate condition in heat transfer problems in *Numer Heat Tr A-Appl* **61** 353-380
- Jagad P I, Puranik B P and Date A W (2015) A novel concept of measuring mass flow rates using flow induced stresses in *Sadhana – Acad P Eng S* **40** 1555-1566
- Jog C S and Pal R K (2011) A monolithic strategy for fluid-structure interaction problems in *International Journal for Numer Meth Eng* **85** 429-460
- Kazemi M (2009) Investigation of fluid structure interaction of a head stack assembly in a hard disk drive in *IEEE T Magn* **45** 5344-5351
- Keramat A, Tijsseling A S, Hou Q and Ahmadi A (2012) Fluid-structure interaction with pipe-wall viscoelasticity during ... *J Fluid Struct* **28** 434-455
- Matthies H G and Steindorf J (2003) Partitioned strong coupling algorithms for fluid-structure interaction in *Comput Struct* **81** 805-812
- Papadakis G (2008) A novel pressure-velocity formulation and solution method for fluid-structure interaction problems in *J Comput Phys* **227** 3383-3404
- Park K C, Felippa C A and Ohayon R (2001) Partitioned formulation of internal fluid-structure interaction problems by localized lagrange multipliers in *Comput Meth Appl Mech Eng* **190** 2989-3007
- Peng W, Zhang Z Y, Gogos G and Gazonas G (2011) Fluid structure interactions for blast wave mitigation in *J Appl Mech-T ASME* **78** 1-8
- Peskin C S (1972) Flow patterns around heart valves: A numerical method in *J Comput Phys* **10** 252-271
- Peskin C S (2002) The immersed boundary method in *Acta Numerica* **11** 479-517
- Piperno S, Farhat C and Larrouturou B (1995) Partitioned procedures for the transient solution of coupled aroelastic problems Part: I Model problem, theory and 2-dimensional application in *Comput Method Appl M and Engineering* **124** 79-112
- Ryzhakov P B, Rossi R, Idelsohn S R and Onate E (2010) A monolithic lagrangian approach for fluid-structure interaction problems in *Comput Mech* **46** 883-899
- Schafer M, Teschauer I, Kadinski L and Selder M (2002) A numerical approach for the solution of coupled fluid-solid and thermal stress problems in crystal growth processes in *Comp Mat Sci* **24** 409-419
- Svacek P (2011) Numerical approximation of flow induced vibrations of channel walls in *Comput Fluids* **46** 448-454
- Takagi S, Sugiyama K, Ii S, and Matsumoto Y (2012) A review of full eulerian methods for fluid structure interaction problems in *J Appl Mech-TASME* **79** 010911-843
- Takizawa K and Tezduyar T E (2011) Multiscale space-time fluid-structure interaction techniques in *Comput Mech* **48** 247-267
- Tang D L, Yang C, Kobayasi S, Zheng J and Vito R P (2003) Effect of stenosis asymmetry on blood flow and artery compression: A three-dimensional fluid-structure interaction model in *Ann Biomed Eng* **31** 1182-1193
- Tezduyar T E, Behr M and Liou J (1992) A new strategy for finite-element computations involving moving boundaries and interfaces - the deforming-spatial-domain space-time

- procedure Part: I The concept and the preliminary numerical tests in *Comput Method Appl M* **94** 339-351
- Tezduyar T E and Sathe S (2007) Modelling of fluid-structure interactions with the space-time finite elements: Solution techniques in *Int J Numer Meth Fl* **54** 855-900
- Unger R, Haupt M C, Horst P and Radespiel R (2012) Fluid-structure analysis of a flexible flapping airfoil at low reynolds number flow in *J Fluid Struct* **28** 72-88
- van Loon R, Anderson P D, van De Vosse F N and Sherwin S J (2007) Comparison of various fluid-structure interaction methods for deformable bodies in *Comput Struct* **85** 833-843
- von Scheven M and Ramm E (2011) Strong coupling schemes for interaction of thin-walled structures and incompressible fluids in *Int J Numer Meth Eng* **87** 214-231
- Wen C Y, Yang A S, Tseng L Y and Tsai W L (2011) Flow analysis of a ribbed helix lip seal with consideration of fluid-structure interaction in *Comput Fluids* **40** 324-332
- Yu P, Yeo K S, Sundar D S and Ang S J (2011) A three-dimensional hybrid meshfree-cartesian scheme for fluid-body interaction in *Int J Numer Meth Eng* **88** 385-408.